A 3-D Deformable Surface Method for Automatic Hippocampus-Amygdala Complex Segmentation

M. M. Karimi, N. Batmanghelich, H. Soltanian-Zadeh, *Senior Member, IEEE,* and C. Lucas

Abstract-- **In this paper, we propose an atlas-based method for hippocampus-amygdala complex segmentation. An atlas is registered on all subjects and its transformation is calculated for each subject. This transformation is applied to the structural segmentation of the complex in atlas to construct an initial surface for the hippocampus-amygdala complex of each subject. A possibility approach is introduced for the segmentation process. Two different kinds of deformation based on edges and information obtained from tissue segmentation are used to find different parts of the complex. A new energy is defined to use tissue information. This energy is adopted to expand the model to embed dominant gray matter points in the volume and also withdraw from dominant white matter and CSF points. The initial shape is divided into several parts. In the normal direction of the center of each part, we construct a profile which search for the best point that maximizes this new energy. This algorithm is reliable for finding the overall shape of the complex. It overcomes the poor features of the complex such as weak edges and noise. The algorithm is examined on 5 different subjects and validated using two different validation methods.**

I. Introduction

THE amygdala is an almond-shaped structure, which is situated anterior and partly superior to the tip of the temporal horn of the lateral ventricle [1]. The hippocampus is a cylindrical structure, voluminous interiorly, extending as much as 4-5 cm from the tip of the temporal horn to the splenium of the corpus callosum where it becomes continuous with the fornix. The hippocampus commonly is divided into three parts: head, body, and tail [2].

In the coronal view of the brain images, the boundary between hippocampus and amygdala is often indistinct. In fact, amygdala and hippocampus are separated with the landmarks of temporal horn of lateral ventricle. These landmarks usually are so vague and tolerable that even for an expert, it is impossible to say where the exact boundary between amygdala and hippocampus is. However, this boundary may be seen more clearly in sagittal views. One way to distinguish these two structures is to segment these structures in sagittal slices from each other and then cut the volume in the coronal view. The points obtained from the previous stage of segmentation in the sagittal view appear in the coronal view and make the boundary between amygdala and hippocampus [1]. Because the boundary between amygdala and hippocampus is not apparent in our data set, we segment the whole complex of these structures altogether.

We use a deformable surface for this purpose. A powerful method for finding an object in a 3D image is deformable surface [3], [4]. This surface moves towards the desired object with information extracted from the geometrical features (internal forces) and information obtained from the edges and grayscales of the image (external forces) [3]. When the image includes noise or weak edges, such as hippocampus-amygdala complex, the model should move toward the target passing weak edges and partial volumes [5].

We propose a method to solve this problem using information obtained from the tissue segmentation. We introduce three kinds of deformation each one having a kind of effect in the deformation process.

II. METHODOLOGY

The simplex meshes model is used as the basis of our model. The simplex meshes model is a 3-D deformable surface, which was initially used as a representation and later for segmentation purposes [6].

As seen in Fig.1 each vertex of the simplex mesh has only

Mohammad Mehdi Karimi is with the control and intelligent processing center of excellence, Department of Electrical and Computer Engineering, University of Tehran, Tehran 14395-515, Iran. (email: m.karimi@ece.ut.ac.ir)

Nematollah Batmanghelich is with the control and intelligent processing center of excellence, Department of Electrical and Computer Engineering, University of Tehran, Tehran 14395-515, Iran. He is also with the Institute for Studies in Theoretical Physics and Mathematics, Tehran, Iran (email: k.batman@ece.ut.ac.ir)

Hamid Soltanian-Zadeh is with the Department of Radiology, Henry Ford Health System, Detroit, MI 48202 USA. He is also with the control and intelligent processing center of excellence, Department of Electrical and Computer Engineering, University of Tehran, Tehran 14395-515, Iran. (email: hamids@rad.hfu.edu)

Caro Lucas is with the control and intelligent processing center of excellence, Department of Electrical and Computer Engineering, University of Tehran, Tehran 14395-515, Iran. He is also with Institute for Studies in Theoretical Physics and Mathematics, Tehran, Iran. (email: lucas@ipm.ir)

0-7803-8701-5/04/$20.00 (C) 2004 IEEE

three neighbors. We use this model because the calculation of the normal vector and curvature is straight-forward and can be extracted from any triangulation algorithm using duality property between simplex meshes and triangulation [7].

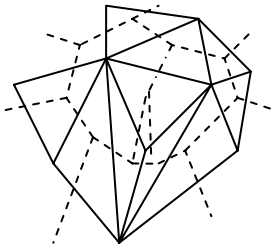

Fig. 1. Duality between triangulation and simplex meshes. Solid lines are lines of triangulation.

As mentioned before, in this model each vertex is connected to three neighbors. The normal vector at each vertex is computed as:

$$\mathbf{n}_i = \frac{\mathbf{P}_{N_1(i)} \times \mathbf{P}_{N_2(i)} + \mathbf{P}_{N_2(i)} \times \mathbf{P}_{N_3(i)} + \mathbf{P}_{N_3(i)} \times \mathbf{P}_{N_1(i)}}{\left\| \mathbf{P}_{N_1(i)} \times \mathbf{P}_{N_2(i)} + \mathbf{P}_{N_2(i)} \times \mathbf{P}_{N_3(i)} + \mathbf{P}_{N_3(i)} \times \mathbf{P}_{N_1(i)} \right\|} \qquad (1)$$

where the positions of the three neighbors of *i*-th vertex are shown by $\mathbf{P}_{N_1(i)}, \mathbf{P}_{N_2(i)}, \mathbf{P}_{N_3(i)}$ (see Fig. 2).

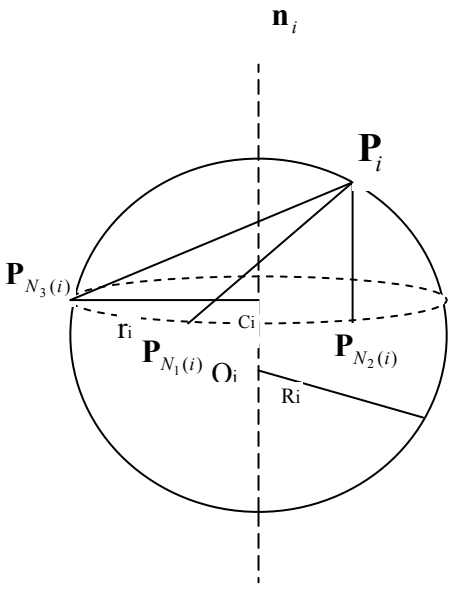

Fig. 2. A typical vertex with its three neighbors.

The segmentation process consists of the following steps:

1) Initialization: This is the first step of the deformation that has a fundamental role in deformation process. In this step, a deformable surface is put near the hippocampus-amygdala complex. The more adjacent to the border, the better segmentation result. An atlas-based method is used for this purpose. We use SPM (statistical parametric mapping) toolbox [8] as a registration tool and project a structural segmentation of the complex on the subject's MRI. This uses an affine transform obtained from the atlas registration to each subject. Because we do not use nonlinear transformations, in some parts of the initial complex, the model deviates greatly from the desired structure. Thus, an erosion algorithm is done on the initial shape on each slice and then we construct the initial surfaces.

2) Initial model: After initialization, an isosurface algorithm is applied on the initial shape and triangulation model of the surface is extracted.

3) Simplex meshes model: From duality property between simplex meshes and triangulation [7], vertices and faces of simplex meshes are extracted. (see Fig. 1)

4) Deformation: After construction, the model must deform. Three kinds of deformation are proposed:

A) Deformation based on a new gradient-based force that pulls different parts of the model with its related vertices to the desired edges. This force is defined as:

$$\mathbf{F}_i = \sum_{j=1}^{J} u_{ij} (\mathbf{F}_{ex,j} \cdot \mathbf{n}_j)\ \mathbf{n}_j \qquad (2)$$

where *j* depicts the cluster or part number and *i* is the vertex number. For each cluster, we find the center of the cluster ($\mathbf{S}_j$) and the normal vector is computed at the center of each cluster ($\mathbf{n}_j$). For each vertex, a fuzzy membership function is introduced which determines the membership of each vertex to each cluster (u_{ij}). We use Euclidean distance ($d(\mathbf{P}_i, \mathbf{S}_j)$) for the definition of u_{ij}:

$$u_{ij} = \frac{1}{1 + d(\mathbf{P}_i, \mathbf{S}_j)} \qquad (3)$$

The position of vertex *i* is represented by $\mathbf{P}_i$ and $\mathbf{F}_{ex,j}$ is an external force which is defined in [3] and enforced on the center of the j-th cluster:

$$\mathbf{F}_{ex,j} = \nabla^2 (I(x_j, y_j, z_j) * G_\sigma) \qquad (4)$$

No internal forces are defined in this kind of deformation because the curvature continuity constraint will be satisfied with this special kind of deformation. Each vertex moves in the direction of the normal vector of the part that this vertex has the largest membership to it. This makes different parts of the model move smoothly. For each vertex, we have:

$$\mathbf{P}_i^{t+1} = \mathbf{P}_i^t + \beta \cdot \mathbf{F}_i \quad (5)$$

where $\mathbf{P}_i^{t+1}$ is the position of the *i*-th vertex in *t+1* iteration and β is the factor that determines the rate of deformation.

B) The second kind of deformation is based on tissue segmentation. Using FSL (fMRI Software Library) software [9] each brain is segmented into 3 separate volumes of gray matter, white matter and CSF. In each part of the model that must deform with this method, a profile is constructed at the position of the vertex that is representative of that part. This profile is constructed in the normal direction of this vertex and has 7 points. We search in the direction of this profile to find the point that maximizes the following energy function:

$$E = \sum_{i=1}^{N} (GM_i - WM_i - CSF_i) \quad (6)$$

where *N* is the number of points embedded inside volume and GM_i, WM_i, CSF_i are the gray level of segmented gray matter, white matter and CSF in each point. This energy is adopted to expand the model to embed more dominant gray matter points in the volume and withdraws from dominant white matter and CSF points. In the direction of each profile, we change the position of the center of each part. The positions of the vertices change according to the following equation:

$$\mathbf{P}_{i,k}^{t+1} = \mathbf{P}_{i,k}^{t} + u_{ij} \cdot (k-4) \cdot \mathbf{n}_j \quad (7)$$
$$k = 1,2,...,7$$

where $\mathbf{P}_{i,k}^{t}$ is the position of the *i*-th vertex when the center of the *j*-th cluster or part moves to the *k*-th point of its normal profile. After each step of the search, we find the energy defined in equation (6) and is related to move the center of the *j*-th part to *k*-th point of its profile. In each step of search on this profile, some points may add or subtract from the points embedded by the surface and *N* may change. If a part of the model is in a CSF or white matter dominant region, the model tries to increase energy by going to the point on the profile that eliminates these points. If it is in the gray matter dominant region, it will be expanded to embed more dominant gray matter points. The point which has the maximum energy among these 7 points is selected as the target point and the model deforms to this point. To avoid redundant calculations, we use a threshold value for membership function. It means that if u_{ij} is lower than a threshold value, we do not move its related vertex position at all. This causes the model to deform only in the vicinity of the *j*-th part.

C) After reaching to the vicinity of the complex border, the model moves to the border precisely and will find the details of the border. This step is done similar to the previous deformable models. We use internal forces and external forces defined in [3].

5) From duality property between simplex meshes and triangulation [7], vertices and faces of the triangulation model are extracted. We do this process because we need to visualize the surface as a triangulation model.

6) We use two criteria for validation of the results. One of them is the measurement of the percent of intersection between this method of segmentation and manual segmentation. The Tanimoto measure between two sets **X** and **Y** is defined as:

$$\frac{{}^nX \cap Y}{{}^nX + {}^nY - {}^nX \cap Y} = \frac{{}^nX \cap Y}{{}^nX \cup Y} \quad (8)$$

Because we have the manual segmentation of this complex in each slice separately, we cut the final surface after deformation in each slice, but some vertices fall between two slices in the final surface. If we assign these vertices to the slice more adjacent to them, in the other slice, it may cause discontinuity. Consequently, we define another volume which has a value that determines each voxel has how much membership in the final segmentation. The voxels inside the surface have the value of 1. But the voxels in the vicinity of the border may have any value between 0 and 1 according to the Euclidean distance to the nearest vertices of the model. When we calculate the number of voxels common with manual segmentation, the voxels in the border are counted with their value between 0 and 1.

Another criterion used specially for this complex segmentation is the percent of gray matter inside the surface. Because we use fuzzy tissue segmentation, each voxel in the gray matter volume has a membership between 0 and 1. We add the membership of the vexels that are inside the surface (GM_{int}) and divide it to the number of these points (N). We call it possibility factor (P.F).

$$P.F = \frac{\sum GM_{\text{int}}}{N} \quad (9)$$

III. RESULTS

We applied the proposed method to volume MRI of 5 subjects whose manual expert segmentation of hippocampus and amygdala were also available. This data was obtained from Internet Brain Segmentation Repository (IBSR). Because in some parts of the complex we have weak edges, when the complex deforms just with the forces defined based on gradient, it may be trapped to these weak edges and cannot reach to the strong edges. After 3-D structural projection of the complex to each subject, in each slice with this complex, this part of complex is divided into 8 parts (see Fig. 3). In the superior parts and parts adjacent to the medial and lateral parts of the image, we have partial volumes which produce several layers of weak edges. If initial shape is far from strong edges, it will be trapped to these weak edges. In the inferior parts of the complex, we have a thin layer of white matter that can be detected with gradient based external forces. We found adjacent vertices of deformable surface to the representative of each part. At the inferior parts of the surface, the vertices deform with equation (5) but at the other parts, they deform with

equation (7). Finally, a final tuning was applied on all vertices. The result of deformation is shown in Fig. 4. For validation of the method, we used two criteria. First, we found the percent of intersection between manual segmentation and segmentation using this method. We also validated our method with a possibility factor. Because we knew that this complex is constructed by gray matter, we computed the average of gray matter of all voxels embedded by the deformable surface. Table 1 shows the results of this method for right hippocampus-amygdala complex segmentation of 5 subjects.

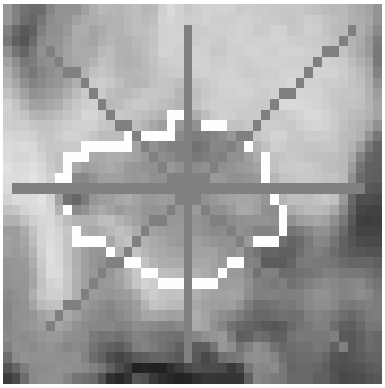

Fig. 3. Intersection of 3-D deformable surface with one slice. Each slice is divided to 8 parts and after that the nearest vertex of the deformable surface is selected as the center of this part.

IV. DISCUSSION

In this paper, we proposed a knowledge-based deformable surface which moves toward target with a multi approach of deformation . We divided this model to separate parts. These parts with their adjacent vertices move toward the desired object. After reaching to the vicinity of the object, we did final tuning on the model. This model has some advantages and disadvantages. Its advantage is that because it uses tissue and edge information simultaneously, it can make a reliable decision. The results confirm this claim. Its disadvantage is that it cannot be extended to the other structures because this method is designed only for this structure and purpose. It is not generic. The other disadvantage of this method is its computational complexity. Because the algorithm must check any changes that occur in the energy function related to the changes of the points of the model, it takes much time to execute. In the future work, we will follow an approach to separate hippocampus and amygdala from each other and also introduce a method to optimize the computational aspects of the algorithm.

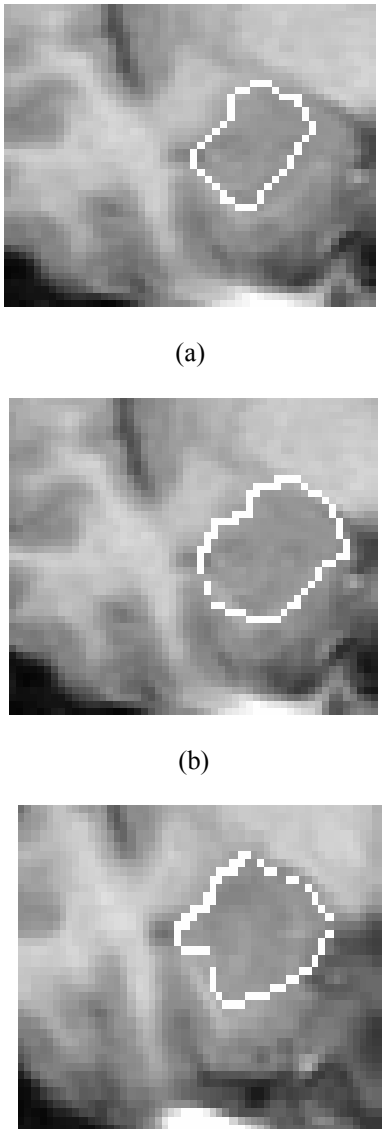

(a) (b) (c)

Fig. 3. Deformation process on slice 61. (a) initial contour after registration (b) final cut of the surface after deformation. (c) manual expert segmentation.

TABLE I
Possibility factor and percent of intersection between manual and automatic segmentations.

Subjects	1	2	3	4	5
Possibility factor	0.84	0.82	0.82	0.83	0.82
Percent of intersection	85%	87%	82%	78%	80%

V. REFERENCES

[1] A. Convit, P. McHugh, O. T. Wolf, M. J. Leon, M. Bobinski, S. Desanti, A. Roche, W. Tsui, "MRI volume of the amygdala: a reliable method allowing separation from the hippocampal formation," *Psychiatry Research: Neuroimaging Section* , vol. 90, pp. 113-123, 1999.

[2] J. C. Tamraz, Y. G. Comair, Atlas of Regional Anatomy of the Brain Using MRI. Berlin: Springer, 2000.

[3] A. Ghanei, H. Soltanian-Zadeh, "A Discrete Curvature-Based Deformable Surface Model with Application to Segmentation of Volumetric Image," *IEEE transaction on information technology in biomedicine,* vol. 6, no. 4, pp. 285-296, December 2002.

[4] H. Delingette, "General object reconstruction based on simplex meshes," *International Jornal of Computer Vision 32,* vol. 1, pp.111-146, 1998.

[5] D. Shen, C. Davatzikos, "A hierarchical Deformable Model Using Statistical and Geometric Information," *IEEE Workshop on Mathematical Methods in Biomdeical Image Analysis (MMBIA2000),* pp. 1-10, South Carolina, 2000.

[6] H. Delingette, "Simplex Meshes: a General Representation for 3D Shape Reconstruction," *Technical Report 2214*, pp.1-70, INRIA, MARCH 1994.

[7] A. Pitiot, H. Delingette, N. Ayache, P. M. Thompson, "Expert Knowledge Guided Segmentation System for Brain MRI," *Medical Image Computing and Computer-Assisted intervention MICCAI'03,* vol. 2879, pp. 644-652, November 2003.

[8] http://www.fil.ion.ucl.ac.uk/spm/

[9] http://www.fmrib.ox.ac.uk/fsl/